W-Band Low-Profile Monopulse Slot Array Antenna Based on Gap Waveguide Corporate-Feed Network

W-Band Low-Profile Monopulse Slot Array Antenna Based on Gap Waveguide Corporate-Feed Network

Abbas Vosoogh, Abolfazl Haddadi, Ashraf Uz Zaman, Jian Yang, Herbert Zirath, *Fellow, IEEE*, and Ahmed A. Kishk, *Fellow, IEEE*

***Abstract*—This paper presents a gap waveguide based compact monopulse array antenna, which is formed with four unconnected layers, for millimeter-wave tracking applications at W-band (85–105 GHz). Recently developed gap waveguide technology removes the need for galvanic contact among metallic layers of waveguide structures, and thereby, makes the proposed antenna suitable for easy and low-cost manufacturing. In this context, a low-loss planar Magic-Tee is designed to be used in a monopulse comparator network consisting of two vertically stacked layers. The gap waveguide planar monopulse comparator network is integrated with a high-efficiency 16×16 corporate-fed slot array antenna. The measured results of the comparator network show the amplitude and phase imbalance values to be less than 0.5 dB and 2°, respectively, over the frequency band of interest. The fabricated monopulse array antenna shows relative impedance bandwidths of 21% with input reflection coefficients better than −10 dB for the sum and difference ports. The null in the difference radiation pattern is measured to be 38 dB below the peak of the sum radiation pattern at 94 GHz. The measured gain is about 30 dBi for the same frequency. The low-loss performance of the comparator network and the feed-network of the proposed array, together with the simple and easy manufacturing and mechanical assembly, makes it an excellent candidate for W-band compact direction-finding systems.**

***Index Terms*—Monopulse antenna, high-efficiency, integration, millimeter-wave, gap waveguide, slot array antenna.**

I. Introduction

Millimeter-wave technologies have been under investigation and development in recent years, in response to the demanding needs for extremely high data rate transmission and highly integrated low-cost and low-power wireless devices for different applications, such as high-definition video, automotive radars, and high-resolution imaging [1]. The huge available bandwidth in the millimeter-wave frequency band (30–300 GHz) represents a great potential in terms of capacity and flexibility. For example, E-band (60–90 GHz) and W-band (75–110 GHz) are attractive for multi-Gbps wireless links and radar systems, due to their low atmospheric absorption, short wavelength, and available bandwidth [2].

Direction finding (DF) techniques are necessary for different millimeter-wave applications, such as finding the position of objects in radar systems, determining the line-of-sight direction in point-to-point wireless links, and detecting the location of unlicensed or undesired radiation sources in security applications. As a technique to measure the direction of arrival of radiation or backscattered wave, monopulse technique has many potential applications, not only in direction-finding, but also in communications, radio astronomy, and sonar [3].

Millimeter-wave monopulse radars are attractive for high-resolution tracking applications. They can provide a narrow beamwidth for high angular accuracy with a relatively small aperture size [4]. To reach a narrow beamwidth for high-gain monopulse tracking radars, reflector antennas are typical candidates, due to their simple design and good performance [5], [6]. However, reflector antennas are bulky due to their three-dimensional structure. Moreover, in millimeter-wave frequencies, the requirements for high surface accuracy (better than $\lambda/20$) for reflectors become more demanding (better than 150 μm at 100 GHz) [7], [8]. Microstrip reflectarray antennas can be a low-profile and low-cost alternative to reflector antennas, and they have been used for W-band monopulse radar systems [9]. However, complicated design, needs for low-loss substrates, and narrow bandwidth are some of the drawbacks of the substrate based reflectarray antennas.

Planar array antennas can provide high-gain performance together with compact and low-profile structure for monopulse applications. The operating bandwidth of an array antenna is mainly limited by its feed-network. Corporate-feeding, which is frequency independent compared to the series feeding, enables a wide bandwidth by in-phase excitation of all radiating elements [10]. Different transmission line technologies can be used to realize planar array antennas for monopulse applications. Hollow waveguide feeding networks introduce no dielectric loss, low conductive loss, and capability to handle high power. The critical challenge of multi-layer hollow waveguide arrays, especially at millimeter-wave frequencies, is achieving good electrical contact among the building blocks of the complicated waveguide structure. Good electrical and galvanic contact can be achieved by using elaborate manufacturing methods, such as diffusion bonding of many thin metal layers [11], which increases fabrication cost and manufacturing complexity [12]. Microstrip lines and Substrate Integrated Waveguides (SIW) are other types of transmission lines, which can be used for a wideband planar array for monopulse applications [13]–[15]. Antennas implemented using these substrate-based transmission lines suffer from low efficiency due to dielectric loss and field leakage in the substrate. The losses can be partly reduced by using low loss dielectrics.

This work is financially supported by the European Research Council (ERC) under the 7th Framework Program ERC grant number 321125.

A. Vosoogh, A. Uz Zaman, and J. Yang are with the Electrical Engineering Department at Chalmers University of Technology, Gothenburg, Sweden (e-mails: abbas.vosoogh@chalmers.se).

A. Haddadi is with Gapwaves AB, Gothenburg, Sweden.

H. Zirath is with the Department of Microtechnology and Nanoscience, Chalmers University of Technology, Gothenburg.

A. A. Kishk is with the Electrical and Computer Engineering Department, Concordia University, Montreal, Canada.

The gap waveguide technology, firstly proposed in [16] and [17], is a guiding structure that can achieve low-loss performance, manufacturing flexibility, and cost effectiveness as well as no need for galvanic contact among the different building blocks of the waveguide structure. In gap waveguide technology the direction of propagation of the wave is controlled by using a guiding structure such as ridge [17] or inverted microstrip line [18] in parallel-plate waveguide configuration. A periodic electromagnetic bandgap (EBG) structure, i.e. a pin texture, around the guiding structure eliminates any possible leakage and higher order modes. The EBG structure also can be used to form the guiding structure, for example in groove gap waveguide [19]. Different millimeter-wave devices such as antennas [12], [20]–[25], filters [26]–[32], and diplexers [33]–[36] have been reported with good performance based on this new technology. Moreover, different fabrication techniques such as Computer Numerical Control (CNC) machining [20], [37], die-sink Electric Discharge Machining (EDM) [22], Direct Metal Laser Sintering (DMLS) 3D printing [38], [39], and printed circuit board technology (PCB) [24], [25], suggest flexible manufacturing methods with affordable cost.

In this paper, we present the integration of a wideband planar monopulse comparator network with a high-gain corporate-fed slot array antenna based on gap waveguide technology. The proposed module has a novel and flexible architecture with high-efficiency and wide impedance bandwidth (85–105 GHz). The proposed monopulse antenna is formed by four unconnected layers. There is no need for electrical and galvanic contact among the layers, and this makes the antenna easier to manufacture and assemble mechanically. All these features make the proposed antenna a suitable candidate for 2-D (*E*- and *H*-planes) tracking applications at W-band. In Section II the design of the Magic-Tee using gap waveguide transmission line is presented. Designing the comparator network based on the presented Magic-Tee is another part of this section. The design of the radiating unit cell and the integration of the monopulse comparator network with the feed-network of a 16×16 array antenna is presented in Section III. Experimental results and a comparison with several published works on different technologies are given in Section IV. Finally, Section V gives some concluding remarks.

II. Design of the Monopulse Comparator Network

The key component of any monopulse antenna system is the comparator network. It enables the system to construct the sum and differences patterns. Based on the sum and difference signals, one can find the direction of the target or the electromagnetic emission. Magic-Tees consist of *E*- and *H*-plane T-junctions in 3-D form can be used to construct sum and difference signals in monopulse systems based on hollow waveguides. Fabrication of the 3-D waveguide structure is a challenging task due to the need for perfect electrical contact between the junctions, especially at high frequency.

In this section, we present the design of a planar monopulse comparator network based on gap waveguide technology. In the proposed architecture a comparator network in three distinct layers is formed and stacked on top of each other without any electrical contact requirements.

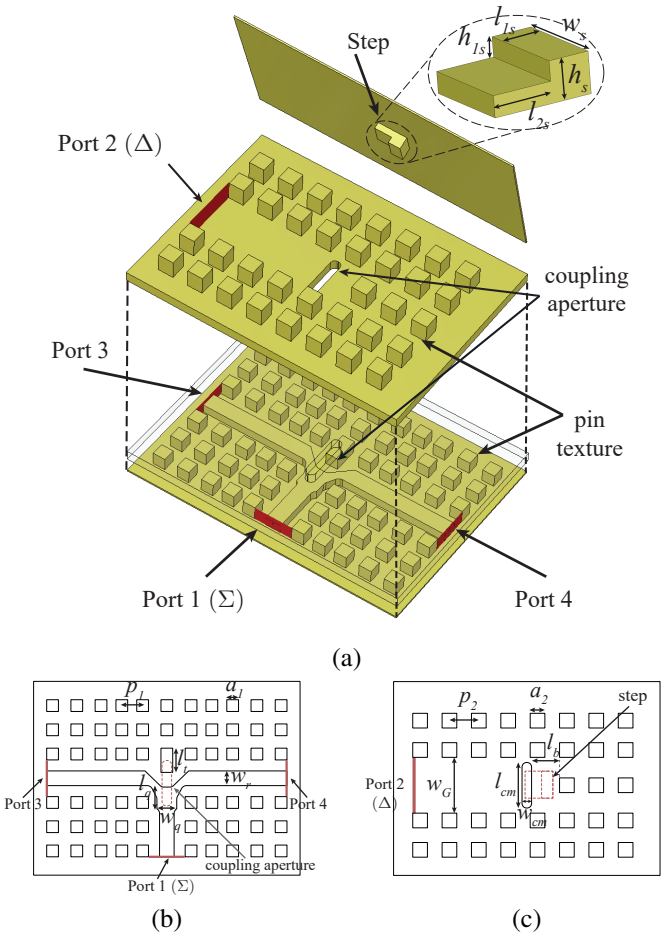

Fig. 1. Proposed planar gap waveguide Magic-Tee. (a) Exploded view. (b) Top view of bottom layer. (c) Top view of the middle layer. (a_1 = 0.65 mm, p_1 = 1.3 mm, l_{1s} = 0.5 mm, l_{2s} = 0.73 mm, h_{1s} = 0.23 mm, h_s = 0.49 mm, w_s = 1.2 mm, w_r = 0.65 mm, w_q = 0.88 mm,a_2 = 0.52 mm, d_2 = 0.55 mm, l_t = 1.1 mm, l_q = 1 mm, w_G = 2.5 mm, l_{cm} = 2 mm, w_{cm} = 0.42 mm, l_b = 1.24 mm).

A. Gap waveguide Magic-Tee design

The exploded view of the proposed wideband Magic-Tee is shown in Fig. 1(a). The planar configuration of the Magic-Tee can be used to realize a low-profile comparator network with the capability of easy integration with planar array antennas. The electromagnetic coupling mechanism of the gap waveguide Magic-Tee is similar to the conventional hollow waveguide Magic-Tee.

The proposed Magic-Tee is implemented in three distinct metal layers by combination of *E*- and *H*-planes 3 dB power dividers, as shown in Fig. 1(a). The pin texture acts as a high impedance surface and prevents electromagnetic waves to propagate and leak in undesired directions within a specific frequency band (stopband). Based on gap waveguide concept, all the metal layers are separated by a small gap, and there is no requirement for a metallic contact among the layers, in Fig. 1. Furthermore, electromagnetic waves are guided by forming a groove by using pins on the middle layer and ridges on the bottom layer. All the possible leakages are eliminated by using periodic pins, as an electromagnetic bandgap structure, around the guiding structures.

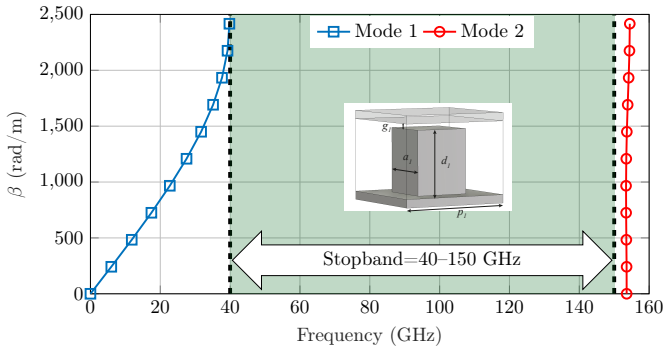

Fig. 2. Dispersion diagram for the infinite periodic pin unit cell. (d_1 = 0.78 mm, a_1 = 0.65 mm, g_1 = 0.07 mm, and p_1 = 1.3 mm)

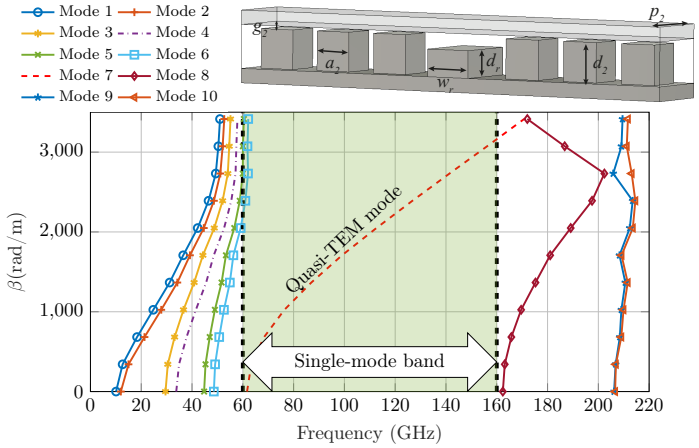

Fig. 3. Dispersion diagram for the infinite ridge and periodic pin unit cell (d_2 = 0.55 mm, a_2 = 0.52 mm, g_2 = 0.03 mm, p_2 = 0.92 mm, d_r = 0.38 mm, w_r = 0.65 mm).

By exciting the Port 3 and Port 4, the sum and difference signals will be constructed in the Port 1 (Σ) and Port 2 (Δ), respectively. A ridge gap waveguide *H*-plane T-junction, on the bottom layer in Fig. 1(b), is used for the sum port. A coupling slot on the middle layer forms an *E*-plane T-junction to subtract the signal at the Port 3 from the signal at the Port 4 and delivers the difference signal to the Port 2. The *E*-plane T-junction on the middle layer is implemented in groove gap waveguide. The reason we have used ridge gap waveguide as the transmission line on the bottom layer is due to the fact that the designed Magic-Tee will be used to implement a comparator network, which itself will integrate with feed-network of an array antenna afterward. The feeding network of the array antenna is in ridge gap waveguide, due to the limited space for corporate feeding.

In the bottom layer, a post with a base length of l_t and a trapezoidal cut in the ridge T-junction are optimized to have wideband impedance matching for the Σ port, as shown in Fig. 1(b). The coupling slot on the middle layer in combination with a step on the top layer acts as an E-plane T-junction for the difference port. The proposed Magic-Tee is optimized by using CST Microwave Studio to have low reflection coefficients at all ports, good isolation between the sum and difference ports, and low amplitude and phase imbalance values at the output ports (Port 3 and Port 4).

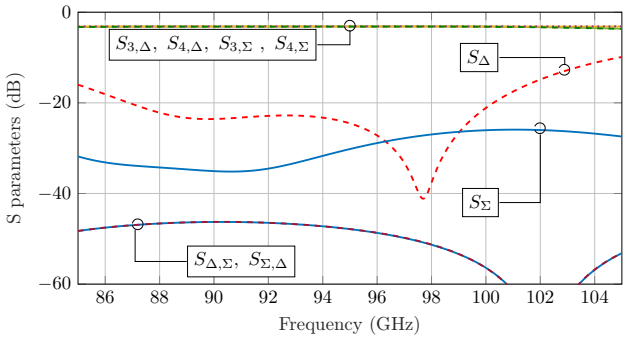

Fig. 4. Simulated performance of the proposed gap waveguide Magic-Tee.

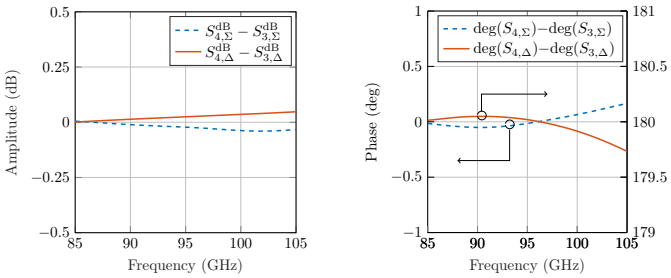

(a) (b)

Fig. 5. Simulated amplitude and phase error at the outputs of the Magic-Tee. (a) Amplitude error. (b) Phase error.

The dispersion diagram of the periodic pin unit cell of the pin texture on the middle layer (Fig. 1(c)) is illustrated in Fig. 2. The pin texture with the given values provides a stopband over the frequency band 40–150 GHz, covering the frequency band of interest. Fig. 2 shows that, even with the presence of a small gap between the pin and the upper plate, there is no propagating mode within the stopband. The pin texture on the bottom layer has a different size from those on the middle layer. On the bottom layer, ridge gap waveguide and smaller pins are used to realize a compact comparator network. Fig. 3 shows the dispersion diagram of the unit cell of a ridge and pins, similar to the one on the bottom layer of the designed Magic-Tee (Fig. 1(b)). A single quasi-TEM mode propagation is achieved over the frequency band of 65–160 GHz.

Fig. 4 shows the simulated performance of the designed Magic-Tee. The sum (Σ) and difference (Δ) ports have reflection coefficients better than −28 dB and −20 dB, respectively, over the frequency band 85–100 GHz. Furthermore, the isolation between the Σ and Δ ports is better than 49 dB. The output ports (Port 3 and Port 4) have about 0.05 dB amplitude imbalance for both the sum and difference input ports. As shown in Fig. 5, the simulated phase imbalance is found to be better than 0.5°. The proposed Magic-Tee shows a wide impedance bandwidth, where the operational bandwidth is mainly limited by the bandwidth of the difference port and the *E*-plane T-junction.

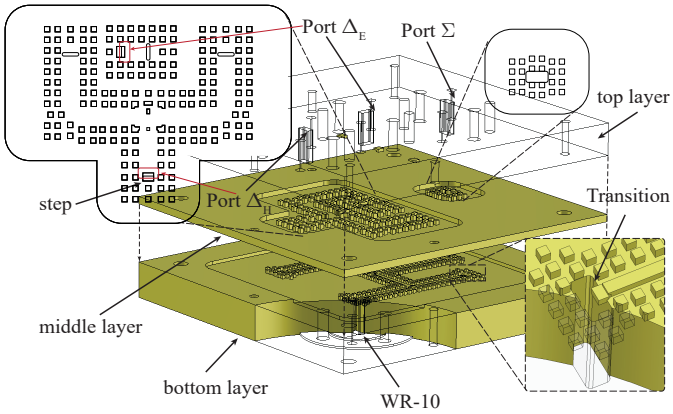

Fig. 6. Configuration of the proposed monopulse comparator network.

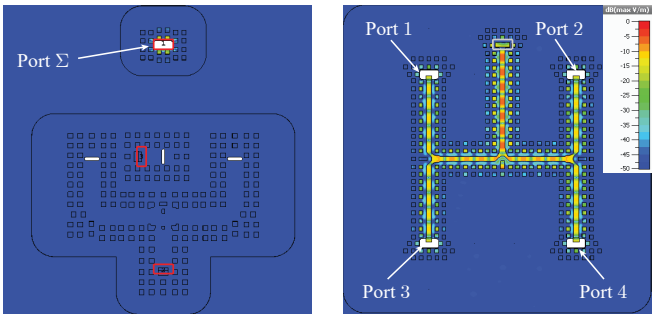

(a) (b)

Fig. 7. Simulated E-field for the sum port at 94 GHz.

B. Monopulse comparator network design

A monopulse comparator network is designed by using the proposed gap waveguide Magic-Tee. Fig. 6 shows the configuration of the comparator network. Three input ports (Ports Σ, Δ_E, and Δ_H) on the top layer deliver sum, *H*-plane, and *E*-plane difference signals, respectively. The energy from the sum port on the top layer is coupled to the ridge feed-network on the bottom layer via a right-angle transition. As the summation happens on the bottom layer and the sum port is placed on the top layer, a pin texture is placed around the sum waveguide on the middle layer to prevent any field leakage since there is a gap between top and middle layers.

The middle and top layers in Fig. 6 will be used in the final monopulse array antenna design in Fig. 17 as Layers 3 and 4, respectively. The bottom layer of the comparator network is used to have four ports to simulate 2-D direction finding performance. Since the designed comparator network is going to be integrated with the feed-network of the array antenna, the pin and ridge dimensions on the bottom layer are similar to those for the antenna feed-network. Simple E-plane probe transitions, similar to the one in [33] are used at the Ports 1–4 to match the quasi-TEM mode of the ridges on the bottom layer to TE_{10} of the standard WR-10 waveguides, as shown in Fig. 6.

Fig. 7 illustrates the simulated electric field on the bottom layer when the Port Σ is excited. In Fig. 7(b), by using two-stage power dividers, the delivered electric fields to the Ports 1–4 are equal in phase and amplitude, or

$$S_{1,\Sigma} = S_{2,\Sigma} = S_{3,\Sigma} = S_{4,\Sigma}.$$

In other words, the summation of the signals from the Ports 1–4 will appear at the Port Σ. Furthermore, Fig. 7(a) shows there is no leakage into the middle layer by exciting Port Σ due to the use of pins around the port opening in the middle layer.

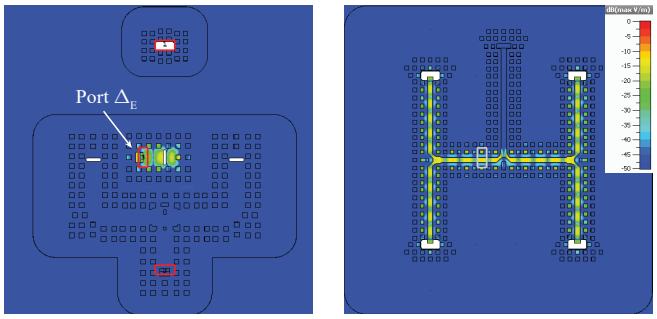

(a) (b)

Fig. 8. Simulated E-field for the *E*-plane difference port at 94 GHz.

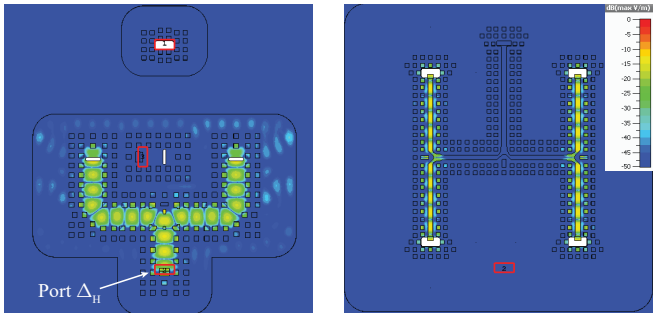

(a) (b)

Fig. 9. Simulated E-field for the *H*-plane difference port at 94 GHz.

Fig. 8 shows the simulated electric field distribution by exciting the Δ_E port. A single Magic-Tee at the center is used in the Δ_E channel. It can be seen in Fig. 8(a) that no field leaks into the Σ and Δ_H channels. Furthermore, fields at the Ports 1 and 3 are out of phase with those at the Ports 2 and 4, with equal amplitudes, or

$$S_{1,\Delta_E} = -S_{2,\Delta_E} = S_{3,\Delta_E} = -S_{4,\Delta_E}.$$

The *H*-plane difference channel consists of two Magic-Tees that are connected via a power divider on the middle layer. The electric field distribution for the wave propagating from the Δ_H port on the top layer to the middle layer is shown in Fig. 9(a). Some field leakage can be seen between the pins and surrounding internal walls, which does not affect the performance since there is no strong leakage into the other channels. Two slots on the middle layer couple the wave into the bottom layer for the *H*-plane difference channel. In Fig. 9(b), all the output Ports 1–4 have equal amplitude with out-of-phase fields at Ports 1, 2 and Ports 3, 4, or

$$S_{1,\Delta_H} = S_{2,\Delta_H} = -S_{3,\Delta_H} = -S_{4,\Delta_H}.$$

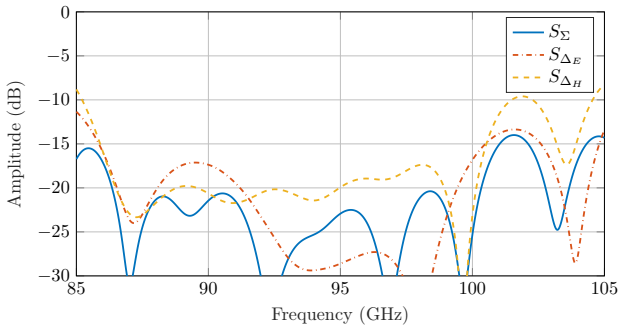

Fig. 10. Simulated reflection coefficients of the designed comparator network.

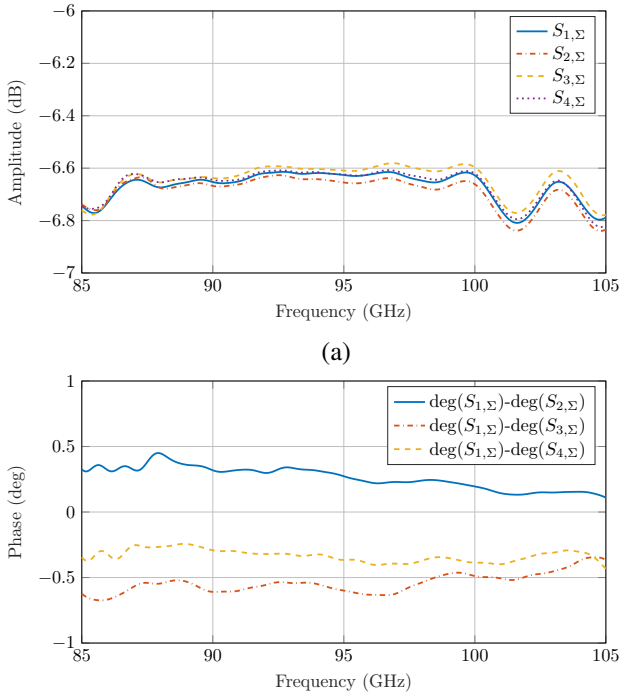

Fig. 11. Sum channel simulated performance. (a) Amplitude, and (b) Phase responses.

Figs. 7, 8, and 9 show that although the building blocks of the designed comparator network are not electrically connected, the electric field is confined within the guiding structures, i.e. ridges and groove. As it mentioned before, it is due to the stopband produced by the periodic pin texture.

The simulated reflection coefficients of the input ports of the designed monopulse comparator network are shown in Fig. 10. All reflection coefficients are better than −15 dB over the frequency band 85–100 GHz. There are some peaks up to −10 dB at some frequencies in $|S_{\Delta_H}|$, which can be due to the groove gap waveguide power dividers and bends in the Δ_H channel.

The amplitude of the transmission coefficients between the output ports and the Σ port are shown in Fig. 11(a). Aluminum is considered as the constructing material of the comparator network in the simulations to take into account the conductive losses. The reflections at the ports and conductive losses in

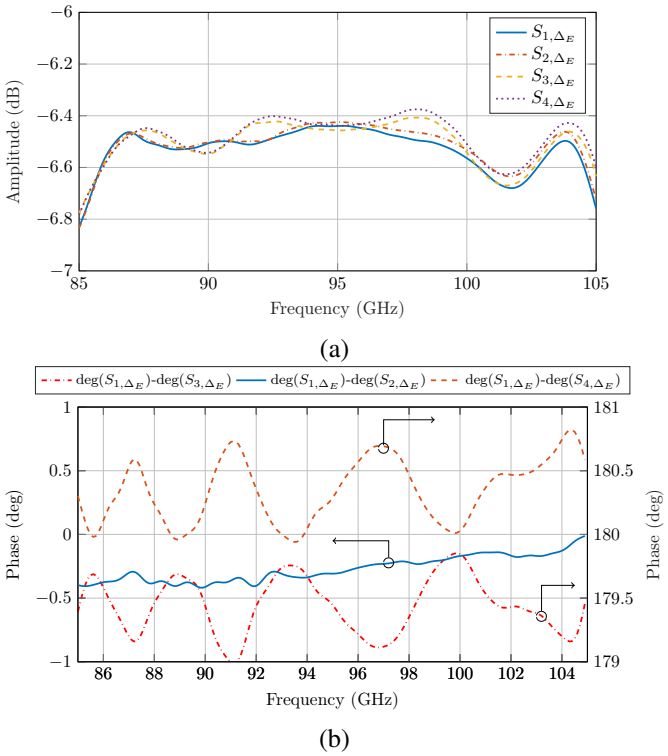

Fig. 12. E-plane channel simulated performance. (a) amplitude, and (b) phase responses.

the ridge gap waveguide do not allow to have the ideal level of −6 dB, and there is a loss of about 0.6–0.8 dB by exciting the sum port. Fig. 11(b) shows the phase imbalance of the transmission coefficient in the sum channel is less than 1°.

The amplitude of the scattering parameters between the Port Δ_E and the Ports 1–4 are illustrated in Fig. 12(a). The simulated insertion loss in the Δ_E channel is about 0.4–0.8 dB. The insertion loss for the Δ_E port is about 0.2 dB less than the one in the Σ port. This is due to the shorter propagation distance in the Δ_E channel. The phase differences between scattering parameters in Fig. 12(b) show that the phase imbalance for in-phase ports (1 and 3) is less than 1°. Furthermore, the phase difference between out-of-phase ports is about 180°±0.5°.

The amplitude of the scattering parameters for transmission from the Δ_H port to the Ports 1–4 are presented in Fig. 13(a). The insertion loss is around 0.4–0.6 dB over the frequency band 87-100 GHz. The lower insertion loss of 0.2 dB for the port Δ_H, in comparison with the Port Σ, is due to having groove gap waveguide in some part of the Δ_H channel. The wave that propagates in the Σ channel is within the ridge gap waveguide network, which has a more conductive loss in comparison with groove gap waveguide. The phase error plots for the mentioned scattering parameters are shown in Fig. 13(b). The phase imbalances for in-phase and out-of-phase ports are better than 1°.

For a high-performance monopulse system, the sum and difference ports should be highly isolated. As stated before, a proper design of the pin textures allows preventing any leakage between the neighbor channels. Fig. 14 shows that the isolation

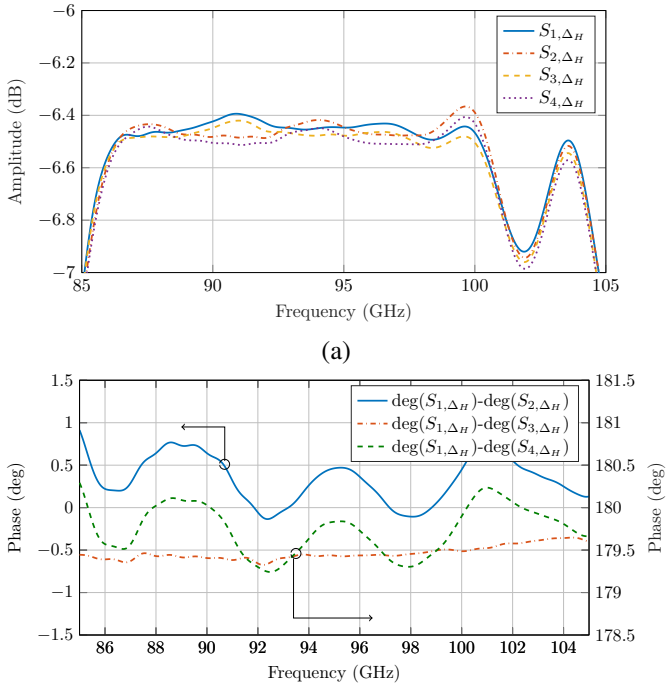

Fig. 13. *H*-plane channel simulated performance. (a) Amplitude, and (b) Phase responses.

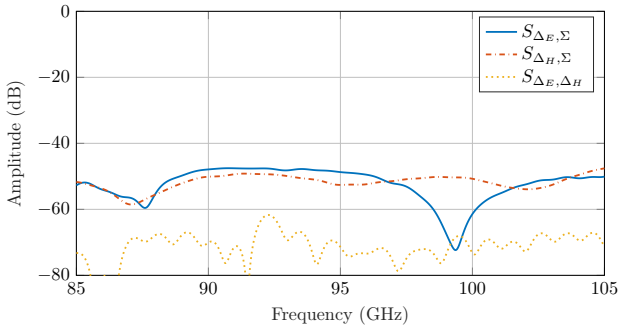

Fig. 14. Simulated isolation between the input ports of the designed comparator network.

between the sum port and each of the difference ports ($S_{\Delta_E,\Sigma}$ and $S_{\Delta_H,\Sigma}$) are better than 50 dB. Moreover, isolation better than 60 dB has been achieved between the two difference ports (S_{Δ_E,Δ_H}).

III. Planar Monopulse Array Antenna Design

A 4×4 cavity-backed slot array, as shown in Fig. 15, is designed as subarray for the antenna array. The subarray consists of three unconnected layers, i.e., radiating layer, cavity layer, and feeding layer. Each radiating slot is non-concentrically surrounded by a rectangular cavity on the top, with the height H_{su}, to reduce slot-to-slot coupling. The slots are fed by rectangular cavities to provide a uniform magnetic field on each radiating slot in the unit cell. The radiating slots are rotated by 10° in order to achieve low side-lobe levels on the *E*-, and *H*-planes. The slot rotation can separate the principal radiation planes from the array lattice planes, e.g. *x*-*z*

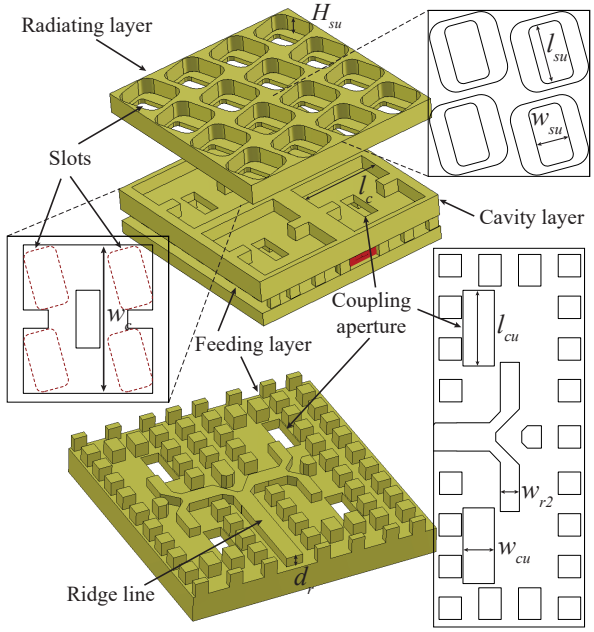

Fig. 15. Gap Waveguide 4 × 4 cavity-backed slot subarray (l_{su} = 1.8 mm, w_{su} = 1 mm, H_{su} = 0.76 mm, w_c = 4.5 mm, l_c = 3.9 mm, l_{cu} = 1.75 mm, w_{cu} = 0.73 mm, w_{r2} = 0.44 mm).

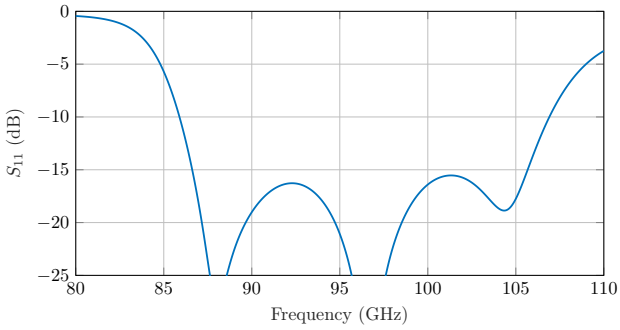

Fig. 16. Simulated reflection coefficient of 4 × 4 slots subarray in infinite array environment.

and *y*-*z* planes, as explained in [12]. Each excited cavity is fed via a coupling slot from a ridge gap waveguide feed network. The unit cell could have been chosen to be 2×2 slots over one feeding cavity without any power divider on the bottom feeding layer, as in [12], [40]. First, a 2×2 cavity-backed slot unit cell is designed using the procedure presented in [12], [40]. Afterward, to consider the loading and mutual coupling of the first two power division stages of the feed- network, as shown in Fig. 15, a 4×4 subarray is re-tuned to achieve wider impedance matching.

A corporate feeding scheme is used to realize a wideband feed-network and excite the radiation slots uniformly with equal phase and amplitude. Ridge gap waveguide is chosen for a low loss and compact feed-network design. Similar design procedure as described in [12], [33] is used to design the feed-network. It should be noted that unequal excitation between the radiating slots can generate grating lobes and degrade aperture efficiency of the array antenna. To prevent unequal excitation of the slots, during the unit cell optimization, the radiation

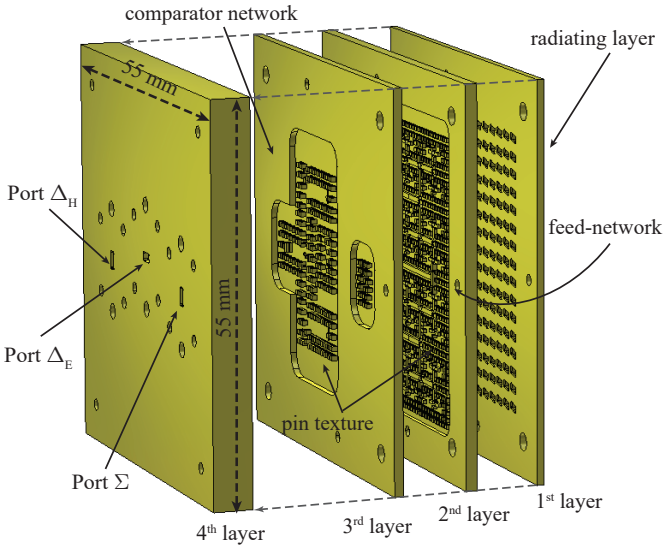

Fig. 17. Detailed description of the proposed monopulse array antenna in four layers.

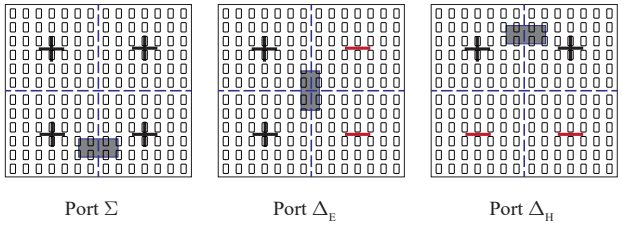

Fig. 18. Operating mechanism of the proposed monopulse array antenna and the position of sum and difference ports.

pattern of a 16×16 array was calculated using the far-field Array Tool in CST MWS to check the array radiation pattern performance.

The simulated reflection coefficient for the optimized 4×4 subarray is shown in Fig. 16. The input reflection coefficient ($|S_{11}|$) is below −15 dB over the frequency band 85–105 GHz. In the simulations, a periodic boundary condition has been used to simulate the subarray in an infinite array environment. Based on the designed and simulated subarray, a 16×16 slot array antenna is designed, and the monopulse comparator network is integrated with the feeding network of the array. The configuration of the array antenna with the integrated monopulse comparator network is shown in Fig. 17.

As shown in Fig. 17, the metal layers are vertically stacked-up on top of each other, which led to a compact integration of the comparator network and the array antenna. The layers do not require a secure electrical contact and can be simply assembled by few screws on the corners. A 16×16 array of radiating slots are adapted on Layer 1, i.e., radiating layer, to achieve about 32 dBi gain. Each 2×2 slots form a subarray and have been fed by a cavity on the top side of Layer 2. Exciting four slots by one cavity helps to reduce the separation between radiating slots and avoid high grating lobes in the corporate feed excitation [41]. An 8×8 array of feeding cavities are excited uniformly by a corporate ridge gap waveguide

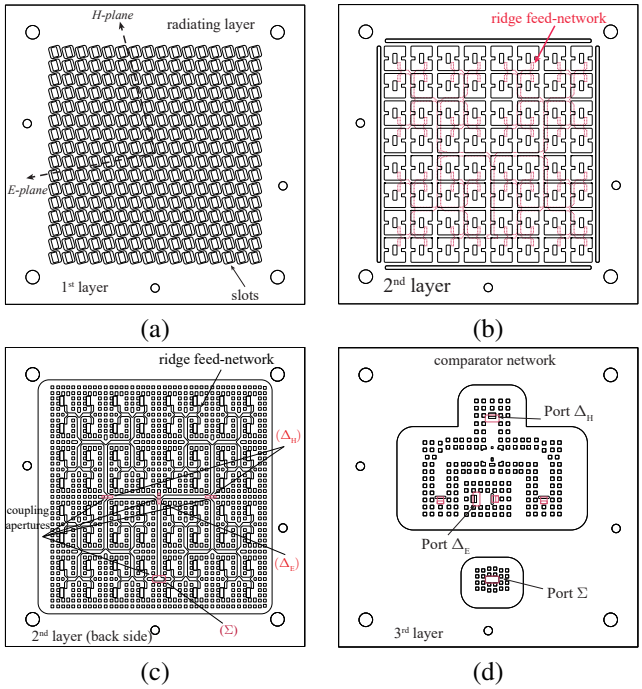

Fig. 19. Configuration of each layer of the proposed monopulse array antenna. (a) Top view of the radiating layer. (b) Top view of Layer 2, consisting of 8×8 cavities to feed the radiating slots. (c) Corporate feed-network on the back side of Layer 2. (d) Top view of the monopulse comparator network.

feed-network on the back of Layer 2. The Layer 3, or the comparator layer, consists of three Magic-Tees to provide two difference signals in the *E*- and *H*-planes, and also a coupling aperture for the sum signal. Finally, Layer 4 contains three ports to excite the sum and difference patterns. Three standard WR-10 flanges are used for all three ports of sum (Port Σ), *H*-plane difference (Port Δ_H), and *E*-plane difference (Port Δ_E). The position of the input ports on the bottom of Layer 4 is shown in Fig. 17.

Fig. 18 shows the operating mechanism and phase distributions among the radiating slots by exciting the different input ports. The slots on Layer 1 radiate with the same phase and generate a sum beam when Port Σ is excited. By exciting Port Δ_E and Port Δ_H half of the antenna's aperture radiates with 180° phase difference and generates difference beams in the *E*-plane and the *H*-plane, respectively. More details of each layer is presented in Fig. 19. The Layer 1, or the radiating layer, has 16×16 radiating slots which are tilted by 10° as shown in Fig. 19(a). The *E*-plane is parallel to the shorter width of the slots. Fig. 19(b) shows the top side of Layer 2 which consists of 8×8 cavities and four corrugations around the rim to avoid any possible leakage from the outer cavities. The ridge corporate feed network on the back side of Layer 2 is also highlighted in Fig. 19(b). The detail of the ridge gap waveguide feed-network is shown in Fig. 19(c). Fig. 19(c) also depicts four coupling slots where one is for the Σ port excitation and the rest are corresponding to the Δ ports on the Layer 3. Fig. 19(d) shows the comparator network, consisting of the Magic-Tees and the power dividers.

For a proper 2-D tracking or direction finding, the proposed monopulse antenna has low reflection coefficients for all ports,

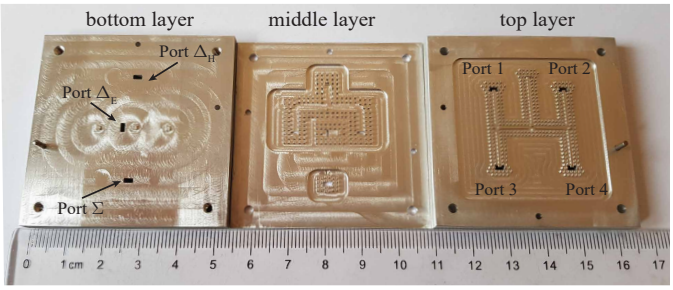

Fig. 20. Fabricated monopulse comparator network array. The layers from left to right are corresponding to the layers from top to bottom in Fig. 6.

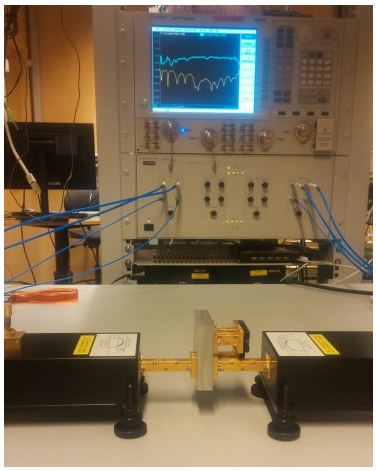

Fig. 21. Measurement setup for the fabricated comparator network.

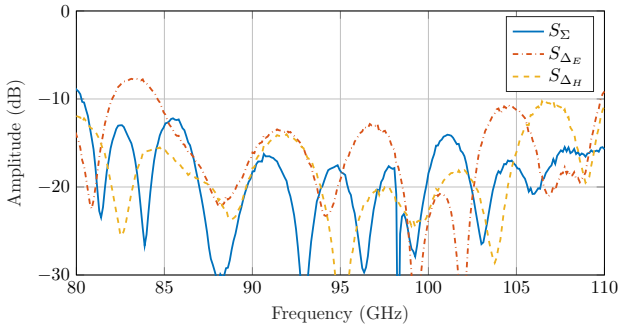

Fig. 22. Measured reflection coefficients of the designed comparator network.

good isolation between the ports, high gain for the sum pattern and deep nulls for the difference radiation patterns.

IV. Experimental Results and Discussion

In order to verify the design procedure and the simulated results, the monopulse comparator network and the integrated module are fabricated by using CNC milling machining in Aluminum. Fig. 20 shows the fabricated comparator network. The fabricated prototype has a simple mechanical assembly, and the metallic layers are simply held in their respective positions by using guiding pins and four screws.

The scattering parameters have been measured by the setup shown in Fig. 21. We have used Keysight N5241A PNA-X and VDI WR-10 extenders to perform the measurements. As

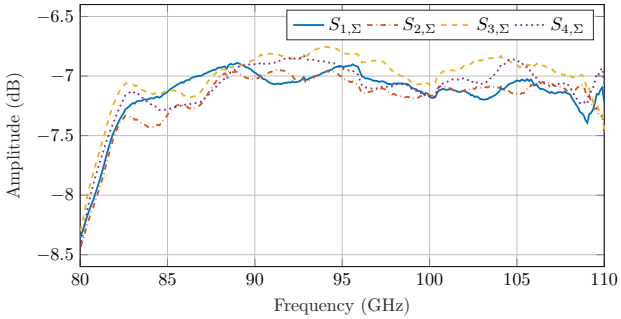

(a)

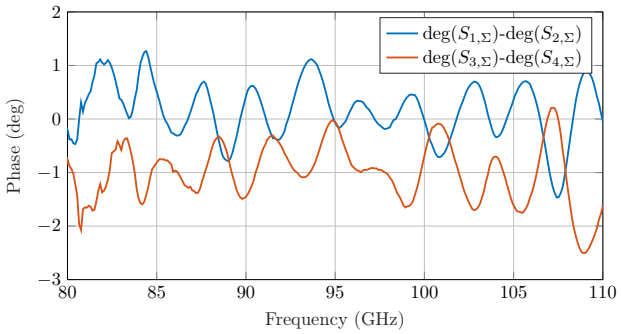

(b)

Fig. 23. Measured transmission coefficients of the sum channel. (a) Amplitude, and (b) Phase responses.

described in Section II, there are seven ports on the comparator network: the Σ, Δ_E, Δ_H input ports on the top layer and the output Ports 1–4 on the bottom layer. Two-port S-parameter measurement has been performed between each input ports and one of the output ports (Ports 1–4), one at the time. Waveguide matched loads are used during each measurement to terminate the other 3 output ports.

The measured reflection coefficients for the Σ and Δ ports are illustrated in Fig. 22. For the frequency band 85–110 GHz, all $|S_\Sigma|$, $|S_{\Delta_E}|$, and $|S_{\Delta_H}|$ are below −12 dB (VSWR = 1.7:1).

The measurement transmission coefficients from the sum channel to the output ports are shown in Fig. 23. The amplitude plots in Fig. 23(a) are about −7 dB for the frequencies higher than 85 GHz. The measured results compared with the simulated one in Fig. 11(a) show around 0.5 dB more losses. This is due to higher mismatch and surface roughness in the fabricated prototype. The measured phase plots in Fig. 22(b) show that phase imbalances in the sum channel is always less than 2° which is close to the simulated value of 1° in Fig. 11(b).

The amplitudes for the measured scattering parameters of the Δ_E and Δ_H channels, are shown in Fig. 24(a) and (b), respectively. The measured values for the $|S_{1,\Delta_E}|$ and $|S_{4,\Delta_E}|$ are shown in Fig. 24. The measured results for the Δ_E channel are between −7 dB and −6.5 dB, which is maximum around 0.2 dB different compared with simulation values in Fig. 12(a). For the Δ_H channel, measured values are between −7.5 dB to −6.5 dB.

The fabricated monopulse array antenna is presented in Fig. 25. The overall size of the manufactured prototype is 55×55×9 mm^3. The manufacturing and assembly process for

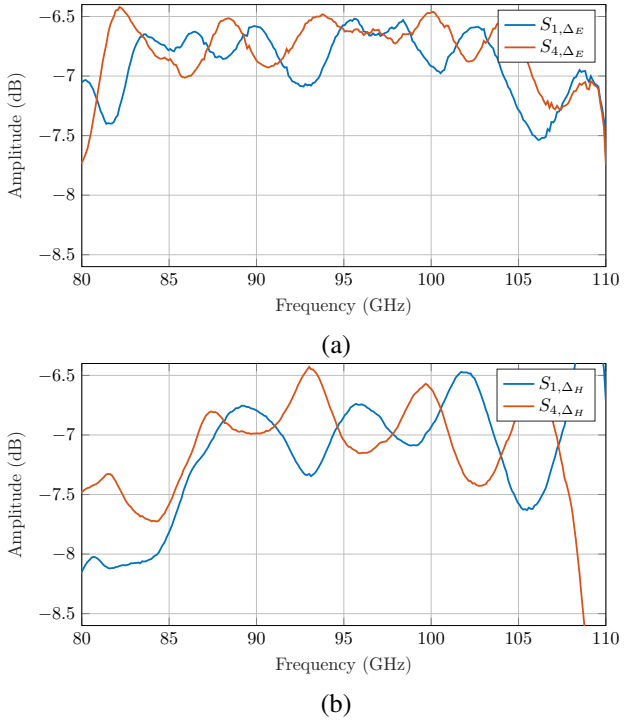

Fig. 24. Measured transmission coefficients of the difference channels. (a) E-plane, and (b) H-plane channels responses.

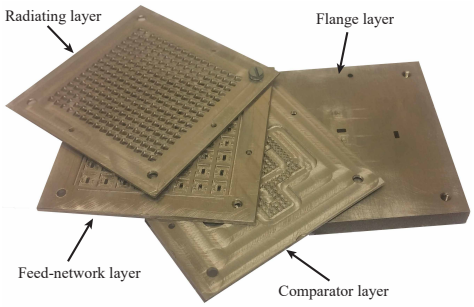

Fig. 25. Photograph of the fabricated planar monopulse array prototype.

the antenna prototype is the same as the comparator in Fig. 20. The simulated and measured reflection coefficients for the sum and difference ports of the fabricated antenna are shown in Fig. 26. The measured results are in good agreement with the simulated ones. The measured reflection coefficient at the Ports Σ, Δ_E, and Δ_H are below -10 dB over the frequency band of 85–105 GHz, except for the Δ_E port at 105 GHz, which goes to -8 dB.

Fig. 27 shows the simulated and measured radiation patterns of the antenna for different frequencies at 90, 95, and 100 GHz at the E-, and H-planes. The radiation characteristics of the antenna are measured in the far-field range test setup. The proposed antenna shows a good radiation pattern with low side-lobe levels in the E-, and H-planes for a wide frequency band. The simulated null in the difference pattern is around 50 dB below the maximum of the sum pattern over the band of interest. However, the measured null is around 40 dB below the maximum of the sum pattern, which could occur due to increased phase and amplitude errors in the comparator

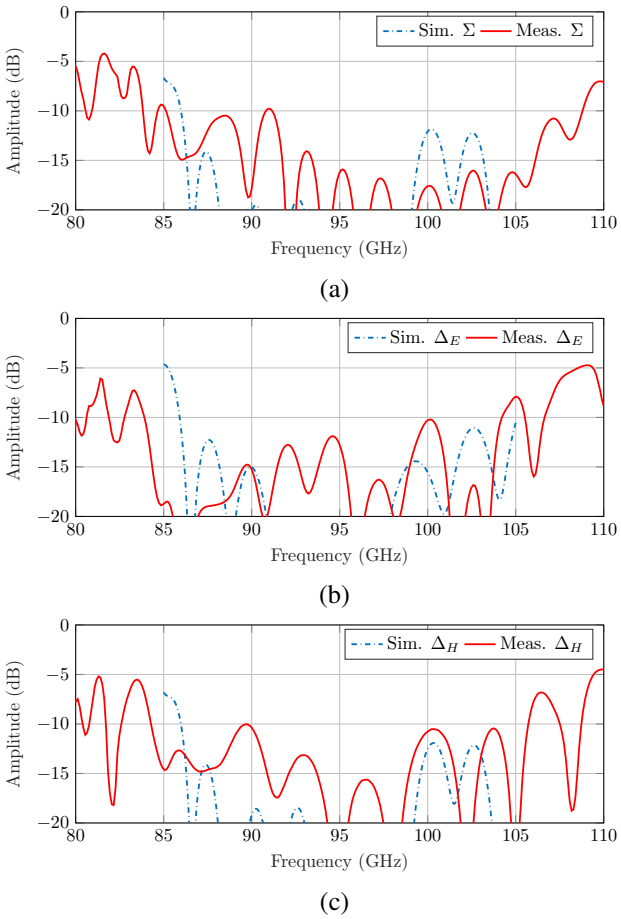

Fig. 26. Simulated and measured reflection coefficients for different ports of the fabricated monopulse antenna: (a) sum, (b) E-plane difference, and (c) H-plane difference port.

network or due to measurement accuracy.

The measured co- and cross-polar gains of the sum pattern at the boresight are shown in Fig. 28. The simulated co-polar gain is higher than 31 dBi with antenna efficiency around 70%. However, due to higher losses in the fabricated antenna, the measured co-polar gain is around 1 dB lower than the simulated one. The drop on the gain at 85 GHz is due to the high reflection coefficient in the sum port. The measured antenna efficiency is more than 50% and around 60% for most of the frequency band. The measured and simulated cross-polar gains are lower than 5 dBi, that gives cross-polar discrimination to be better than 27 dB.

A. *Comparison and discussion*

A comparison between eight published works and the present paper is summarized in TABLE I. Since the present paper is the first gap waveguide-based monopulse antenna, TABLE I shows a comparison between different technologies in terms of scattering parameters (matching and isolation), comparator network parameters (imbalances and loss), and radiation parameters (gain, side-lobes, cross-polarization, and efficiency).

As the proposed antenna benefits from using waveguide-based corporate feeding network, it offers 21% input reflection

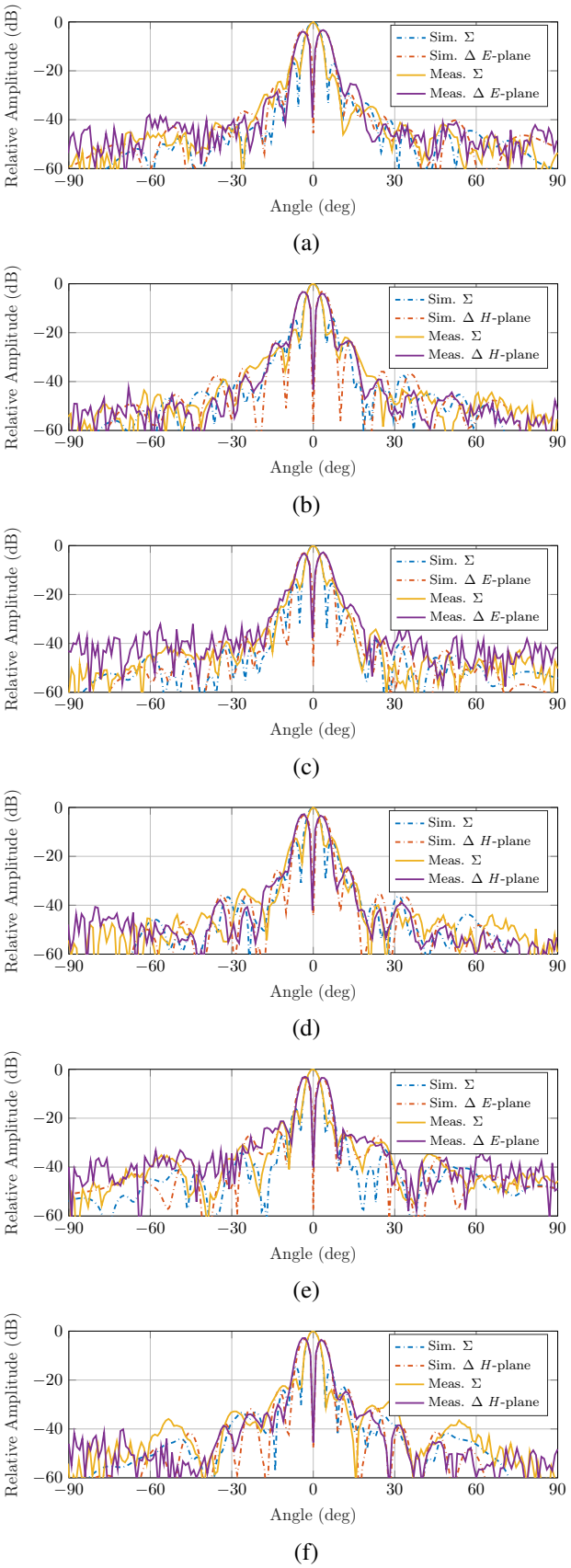

Fig. 27. Simulated and measured normalized sum and difference radiation pattern of the proposed monopulse antenna. (a) *E*-plane at 90 GHz. (b) *H*-plane at 90 GHz. (c) *E*-plane at 95 GHz. (d) *H*-plane at 95 GHz. (e) *E*-plane at 100 GHz. (f) *H*-plane at 100 GHz.

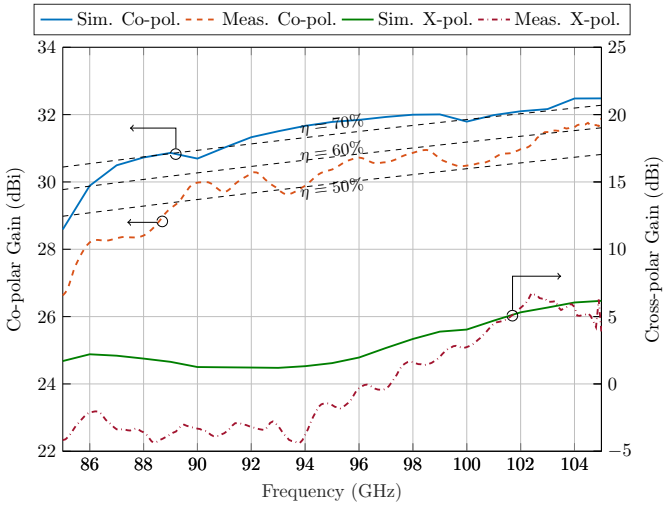

Fig. 28. Simulated and measured gains of the sum beam of the proposed antenna.

coefficient bandwidth. Also, compared to other works, the best isolation (50 dB) between the sum and difference ports has been achieved, which is better than [39] that uses Direct Metal Laser Sintering (DMLS) metal 3D printing. Good isolation in the proposed Magic-Tee makes it possible to have high isolation. It should be noted that due to the limited space between the input ports of the proposed antenna, it was not possible to measure the isolation between the ports. However, by increasing the length of the transmission lines on Layer 3 (see Fig. 19(d)), it is possible to achieve the required separation to accommodate standard flanges without any significant effect on the antenna performance.

The proposed monopulse comparator network in this paper offers a total loss less than 1.5 dB which is close to hollow waveguide design in [39] and lower than PCB- and SIW-based designs in [9], [13], [14]. The measured 1.5 dB loss in the comparator network also contains the first two power division stages of the feed-network. The measured performance of the fabricated comparator network is compared with some available works in TABLE I.

The low-loss comparator and the designed array have enabled the realization of a high-efficiency antenna. TABLE I shows that the efficiency of the proposed antenna system is much higher than PCB-, SIW-, and reflector-based antennas in [5], [6], [9], [13], [14], [42]. The simulated efficiency of the monopulse antenna that is based on hollow waveguide technology in [11] will decrease due to the higher conductive loss after manufacturing. Moreover, in [39] only the aperture efficiency was presented. For the other radiation parameters, like gain, cross-polar level and side-lobe level in the sum pattern, and depth of the null in difference patterns, the proposed antenna parameters are between those based on hollow waveguide designs manufactured by using diffusion bonding and DMLS manufacturing processes.

TABLE I indicates that among all technologies that have been used for manufacturing monopulse antennas, the gap waveguide technology can offer an excellent tracking perfor-

TABLE I
COMPARISON WITH SOME PREVIOUS WORKS ON MONOPULSE ANTENNAS.

Ref.	Structure[1] Manufacturing[2]		Scattering Parameters[3]				Comparator Performance[4]			Antenna Performance[5]					
	Comparator	Antenna	f_0	BW%	VSWR	Iso.	AI (dB)	PI (°)	IL (dB)	XP_Σ	G_Σ	G_Σ-G_Δ	SLL_Σ	ND_Δ	η
[5]	MT n. a.	CA n. a.	93.3	0.65	1.4	20	0.3	0.6	1.1	n. a.	40.1	4	19	27.7	33.1*
[6]	BLC n. a.	CA n. a.	94	4.3	1.4	21	0.2	n. a.	1	23	36.1	5.5	17	50	18
[9]	RR n. a.	MPA PCB	W band	1	n. a.	n. a.	n. a.	n. a.	3.7	32	33	n.a.	20	28	15.5
[11]	MT DB	SAA DB	78.5	21.9	2	n. a.	0.2	n. a.	n. a.	n. a.	32.6	3	13	53	83
[13]	H90 PCB	MPA PCB	14.475	5.6	2	n. a.	n. a.	n. a.	2.93	n. a.	24.5	n. a.	17	30	13.3
[14]	H90 SIW	SAA PCB	94.5	1.60	1.4	n. a.	2.66	n. a.	4.66	n. a.	25.8	3	16	43.7	16.3
[39]	MT DMLS-3DP	SAA DMLS-3DP	15.1	12.9	1.5	30	0.2	1.5	0.15	30	31.5	n. a.	14	30	90*
[42]	BLC n. a.	CA n. a.	92.75	2.5	2	20	0.4	n. a.	n. a.	22	39.6	5.2	15	22.6	51.9
This work	MT GWT	SAA GWT	95	21	2	50	0.5	2	1	27	30.5	3	20	40	60

[1] Structures: RR: Rat-Race, MPA: Microstrip Patch Array, H90: 90-degrees 3-dB Hybrid, MT: Magic-Tee, BLC: Branch-Line Coupler, SAA: Slot Array Antenna, CA: Cassegrain Antenna.
[2] Manufacturing technologies: PCB: Printed Board Circuit, DB: Diffusion Bonding, DMLS-3DP: DMLS 3D Printing, GWT: Gap Waveguide Technology, n. a.: not assigned.
[3] Parameters: f_0: center Frequency in GHz, BW%: relative Band-Width in percent, Iso.: Isolation between Σ and Δ ports.
[4] AI: Amplitude Imbalance, PI: Phase Imbalance, IL: Insertion loss in comparator.
[5] XP_Σ: co- to cross-polar level for Σ pattern in dB, G_Σ: Gain for Σ pattern in dBi, G_Σ-G_Δ: difference between Gain for Σ and Δ pattern in dB, SLL_Σ: peak gain to first Side-Lobe Level for Σ pattern in dB, ND_Δ: Null-Depth in Δ pattern with respect to Σ pattern in dB, η: antenna efficiency in percent.
* Aperture efficiency

mance in broader bandwidth, higher gain and efficiency, lower cross-polar level, and deeper null in W-Band, together with a low cost and easy assembly process.

In order to improve the efficiency of the manufactured antenna, the effective surface conductivity should be increased. Regarding the material selection, silver-plating can be used to improve the electrical conductivity by a factor of 2. On the other hand, surface roughness can also increase ohmic loss. Based on Gold-Helmreich model for effective electrical surface conductivity of rough surfaces [43], considering a surface roughness of about 1 μm for a milled aluminum surface, the effective surface conductivity will be reduced by a factor of 4 compared to ideally smooth one. Therefore, surface treatments to have a better surface smoothness of the milled antenna can help to increase the surface conductivity.

V. Conclusion

A low-profile, broadband and high-efficiency monopulse slot array antenna has been designed for tracking applications at W-band, covering 85–105 GHz frequency band. The antenna has been constructed from four distinct layers, consisting of a monopulse comparator network, and a 16×16 slot array antenna. The use of the gap waveguide technology has eliminated the need for galvanic contact between the different layers, which has facilitated manufacturing and assembling the antenna parts. The measured results have been found to be in good agreement with the simulated results for the comparator network as well as for the whole integrated module. Both comparator network and antenna prototypes have been manufactured by CNC machining in Aluminum and layers are assembled and aligned with few screws.

The simulated and measured reflection coefficients of the sum and the difference ports of the comparator network have been achieved better than −15 dB. The measured insertion losses of the sum, *E*- and *H*-plane difference channels have been found to be around 0.5 dB, with the phase imbalance lower than 2° over the frequency band 85–105 GHz. The designed gap waveguide comparator network has been successfully integrated with the corporative feed-network of a 16×16-element cavity-backed slots array antenna. The simulated results have indicated that the monopulse array antenna can reach more than 70% antenna efficiency. However, the measured antenna efficiency has been found to be around 55% due to the higher surface roughness, which led to higher conductive losses in the fabricated prototype.

The return losses for the sum and difference ports of the fabricated antenna are better than 10 dB over the frequency band 85–105 GHz. The simulated and measured radiation patterns, in both *E*- and *H*-planes, have shown a null in the difference pattern of at least 40 dB lower than the peak in the sum pattern, which has a beamwidth of about 4°, and side-lobe level better than 16 dB. Furthermore, The measured cross-polarization has been shown to be better than 27 dB.

The proposed antenna is expected to be a promising candidate for millimeter-wave tracking applications due to its high-performance characteristics in terms of radiation characteristic, isolation and input impedance matching, in addition to its ease of manufacturing and mechanical assembly.

REFERENCES

[1] D. Liu, U. Pfeiffer, J. Grzyb, and B. Gaucher, *Advanced millimeter-wave technologies: antennas, packaging and circuits*. John Wiley & Sons, 2009.

[2] B. Cao, H. Wang, Y. Huang, and J. Zheng, "High-gain L-probe excited substrate integrated cavity antenna array with LTCC-based gap waveguide feeding network for W-band application," *Antennas and Propagation, IEEE Transactions on*, vol. 63, no. 12, pp. 5465–5474, 2015.

[3] S. M. Sherman and D. K. Barton, *Monopulse principles and techniques*. Artech House, 2011.

[4] S. Raman, N. S. Barker, and G. M. Rebeiz, "A W-band dielectric-lens-based integrated monopulse radar receiver," *IEEE Transactions on Microwave Theory and Techniques*, vol. 46, no. 12, pp. 2308–2316, 1998.

[5] Y. Wang, W. Dou, and B. Bi, "W band axially displaced monopulse dual-reflector antenna for inter-satellite communications," *IET Microwaves, Antennas & Propagation*, vol. 10, no. 7, pp. 742–747, 2016.

[6] P. Zheng, G. Q. Zhao, S. H. Xu, F. Yang, and H. J. Sun, "Design of a W-band full-polarization monopulse Cassegrain antenna," *IEEE Antennas and Wireless Propagation Letters*, vol. 16, pp. 99–103, 2017.

[7] A. Haddadi and A. Ghorbani, "Distorted reflector antennas: Analysis of radiation pattern and polarization performance," *IEEE Transactions on Antennas and Propagation*, vol. 64, no. 10, pp. 4159–4167, 2016.

[8] A. Haddadi, A. Ghorbani, and P. Taghikhani, "Distorted reflector antennas: fast and accurate estimation of the surface distortion profile using a new formula," *IET Microwaves, Antennas & Propagation*, vol. 11, no. 9, pp. 1248–1254, 2017.

[9] D. Jahagirdar and J. Prasad, "A W-band trans-twist monopulse microstrip patch reflectarray," in *Radar Conference, 2005. EURAD 2005. European*. IEEE, 2005, pp. 197–199.

[10] T. Tomura, J. Hirokawa, T. Hirano, and M. Ando, "A 45° linearly polarized hollow-waveguide 16×16-slot array antenna covering 71–86 GHz band," *IEEE Transactions on Antennas and Propagation*, vol. 62, no. 10, pp. 5061–5067, 2014.

[11] X. Xu, J. Hirokawa, and M. Ando, "An E-band slotted waveguide monopulse array antenna with corporate-feed using diffusion bonding of laminated plates," in *Antennas and Propagation (ISAP), 2016 International Symposium on*. IEEE, 2016, pp. 308–309.

[12] A. Vosoogh, P.-S. Kildal, and V. Vassilev, "Wideband and high-gain corporate-fed gap waveguide slot array antenna with ETSI class II radiation pattern in V-band," *IEEE Transactions on Antennas and Propagation*, 2016.

[13] H. Wang, D.-G. Fang, and X. Chen, "A compact single layer monopulse microstrip antenna array," *IEEE Transactions on antennas and propagation*, vol. 54, no. 2, pp. 503–509, 2006.

[14] Y. J. Cheng, W. Hong, and K. Wu, "94 GHz substrate integrated monopulse antenna array," *IEEE Transactions on Antennas and Propagation*, vol. 60, no. 1, pp. 121–129, 2012.

[15] T. Li, W. Dou, and H. Meng, "A monopulse slot array antenna based on dual-layer substrate integrated waveguide (SIW)," in *Antennas and Propagation (APCAP), 2016 IEEE 5th Asia-Pacific Conference on*. IEEE, 2016, pp. 373–374.

[16] P.-S. Kildal, "Artificially soft and hard surfaces in electromagnetics," *Antennas and Propagation, IEEE Transactions on*, vol. 38, no. 10, pp. 1537–1544, 1990.

[17] P.-S. Kildal, A. U. Zaman, E. Rajo-Iglesias, E. Alfonso, and A. Valero-Nogueira, "Design and experimental verification of ridge gap waveguide in bed of nails for parallel-plate mode suppression," *IET Microwaves, Antennas & Propagation*, vol. 5, no. 3, pp. 262–270, Feb. 2011.

[18] A. A. Brazález, E. Rajo-Iglesias, J. L. Vazquez-Roy, A. Vosoogh, and P.-S. Kildal, "Design and validation of microstrip gap waveguides and their transitions to rectangular waveguide, for millimeter-wave applications," *Microwave Theory and Techniques, IEEE Transactions on*, vol. 63, no. 12, pp. 4035–4050, 2015.

[19] E. Rajo-Iglesias and P.-S. Kildal, "Groove gap waveguide: A rectangular waveguide between contactless metal plates enabled by parallel-plate cut-off," in *Antennas and Propagation (EuCAP), 2010 Proceedings of the Fourth European Conference on*. IEEE, 2010, pp. 1–4.

[20] A. Vosoogh and P.-S. Kildal, "Corporate-fed planar 60 GHz slot array made of three unconnected metal layers using AMC pin surface for the gap waveguide," *IEEE Antennas and Wireless Propagation Letters*, vol. 15, pp. 1935–1938, Dec. 2015.

[21] ——, "High efficiency 2 × 2 cavity-backed slot sub-array for 60 GHz planar array antenna based on gap technology," in *2015 International Symposium on Antennas and Propagation (ISAP)*. IEEE, 2015, pp. 1–3.

[22] A. Vosoogh, P.-S. Kildal, and V. Vassilev, "A multi-layer gap waveguide array antenna suitable for manufactured by die-sink EDM," in *2016 10th European Conference on Antennas and Propagation (EuCAP)*. IEEE, 2016, pp. 1–4.

[23] A. Vosoogh and P.-S. Kildal, "V-band high efficiency corporate-fed 8× 8 slot array antenna with ETSI class II radiation pattern based on gap technology," in *Antennas and Propagation (APSURSI), 2016 IEEE International Symposium on*. IEEE, 2016, pp. 803–804.

[24] H. Attia, M. S. Sorkherizi, and A. A. Kishk, "60 GHz slot antenna array based on ridge gap waveguide technology enhanced with dielectric superstrate," in *2015 9th European Conference on Antennas and Propagation (EuCAP)*. IEEE, 2015, pp. 1–4.

[25] S. A. Razavi, P.-S. Kildal, L. Xiang, E. Alfonso Alos, and H. Chen, "2 × 2-slot element for 60-GHz planar array antenna realized on two doubled-sided pcbs using SIW cavity and EBG-type soft surface fed by microstrip-ridge gap waveguide," *Antennas and Propagation, IEEE Transactions on*, vol. 62, no. 9, pp. 4564–4573, Sep. 2014.

[26] A. Vosoogh, A. A. Brazález, and P.-S. Kildal, "A V-band inverted microstrip gap waveguide end-coupled bandpass filter," *IEEE Microwave and Wireless Components Letters*, vol. 26, no. 4, pp. 261–263, Apr. 2016.

[27] M. S. Sorkherizi, A. Khaleghi, and P.-S. Kildal, "Direct-coupled cavity filter in ridge gap waveguide," *IEEE Transactions on Components, Packaging and Manufacturing Technology*, vol. 4, no. 3, pp. 490–495, Mar. 2014.

[28] A. Berenguer, M. Baquero-Escudero, D. Sanchez-Escuderos, B. Bernardo-Clemente, and V. E. Boria-Esbert, "Low insertion loss 61 GHz narrow-band filter implemented with groove gap waveguides," in *Microwave Conference (EuMC), 2014 44th European*. IEEE, 2014, pp. 191–194.

[29] E. A. Alós, A. U. Zaman, and P.-S. Kildal, "Ka-band gap waveguide coupled-resonator filter for radio link diplexer application," *IEEE Transactions on Components, Packaging and Manufacturing Technology*, vol. 3, no. 5, pp. 870–879, 2013.

[30] M. S. Sorkherizi and A. A. Kishk, "Fully printed Gap waveguide with facilitated design properties," *IEEE Microwave and Wireless Components Letters*, vol. 26, no. 9, pp. 657–659, 2016.

[31] M. Rezaee, A. U. Zaman, and P.-S. Kildal, "A groove gap waveguide iris filter for V-band application," in *2015 23rd Iranian Conference on Electrical Engineering*. IEEE, 2015, pp. 462–465.

[32] M. S. Sorkherizi and A. A. Kishk, "Completely tuned coupled cavity filters in defected bed of nails cavity," *IEEE Transactions on Components, Packaging and Manufacturing Technology*, 2016.

[33] A. Vosoogh, M. S. Sorkherizi, A. U. Zaman, J. Yang, and A. A. Kishk, "An integrated Ka-band diplexer-antenna array module based on gap waveguide technology with simple mechanical assembly and no electrical contact requirements," *IEEE Transactions on Microwave Theory and Techniques*, vol. 66, no. 2, pp. 962–972, 2018.

[34] M. Rezaee, A. U. Zaman, and P.-S. Kildal, "V-band groove gap waveguide diplexer," in *Antennas and Propagation (EuCAP), 2015 9th European Conference on*. IEEE, 2015, pp. 1–4.

[35] A. Vosoogh, M. S. Sorkherizi, A. U. Zaman, J. Yang, and A. A. Kishk, "An E-band antenna-diplexer compact integrated solution based on gap waveguide technology," in *Antennas and Propagation (ISAP), 2017 International Symposium on*. IEEE, 2017, pp. 1–2.

[36] ——, "Diplexer integration into a Ka-band high-gain gap waveguide corporate-fed slot array antenna," in *Antennas and Propagation & USNC/URSI National Radio Science Meeting, 2017 IEEE International Symposium on*. IEEE, 2017, pp. 2667–2668.

[37] A. U. Zaman and P.-S. Kildal, "Wide-band slot antenna arrays with single-layer corporate-feed network in ridge gap waveguide technology," *IEEE Transactions on Antennas and Propagation*, vol. 62, no. 6, pp. 2992–3001, Jun 2014.

[38] A. Vosoogh, P.-S. Kildal, V. Vassilev, A. U. Zaman, and S. Carlsson, "E-band 3-D metal printed wideband planar horn array antenna," in *Antennas and Propagation (ISAP), 2016 International Symposium on*, 2016.

[39] G.-L. Huang, S.-G. Zhou, and T.-H. Chio, "Highly-efficient self-compact monopulse antenna system with integrated comparator network for RF industrial applications," *IEEE Transactions on Industrial Electronics*, vol. 64, no. 1, pp. 674–681, 2017.

[40] A. Vosoogh, A. U. Zaman, and V. Vassilev, "Wideband cavity-backed slot subarray with gap waveguide feed-network for D-band applications," in *Antennas and Propagation (EUCAP), 2017 11th European Conference on*. IEEE, 2017, pp. 207–209.

[41] T. Tomura, Y. Miura, M. Zhang, J. Hirokawa, and M. Ando, "A 45° linearly polarized hollow-waveguide corporate-feed slot array antenna in the 60-GHz band," *Antennas and Propagation, IEEE Transactions on*, vol. 60, no. 8, pp. 3640–3646, 2012.
[42] P. Zheng, B. Hu, S. Xu, and H. Sun, "A W-band high-aperture-efficiency multipolarized monopulse cassegrain antenna fed by phased microstrip patch quad," *IEEE Antennas and Wireless Propagation Letters*, vol. 16, pp. 1609–1613, 2017.
[43] G. Gold and K. Helmreich, "A physical surface roughness model and its applications," *IEEE Transactions on Microwave Theory and Techniques*, vol. 65, no. 10, pp. 3720–3732, 2017.

Abbas Vosoogh received the B.Sc. degree in electrical engineering from the University of Sistan and Baluchestan, Zahedan, Iran, and the M.Sc. degree from K. N. Toosi University of Technology, Tehran, Iran, in 2008 and 2011, respectively. He is currently pursuing his Ph.D. degree with Chalmers University of Technology, Gothenburg, Sweden. His current research interests include the development of gap waveguide technology for millimeter and submillimeter wave applications, microwave passive components, EBG, soft and hard surfaces, mm-wave planar array antennas, and integration of passive and active components with array antenna.

Mr. Vosoogh was a recipient of the Best Student Paper Award of the 2015 International Symposium on Antennas and Propagation, TAS, Australia, the CST University Publication Award 2016, the Best Paper Award and the Best Student Paper Award of the 2016 International Symposium on Antennas and Propagation, Okinawa, Japan, and the First Prize Student Award of the 2017 IEEE International Symposium on Antennas and Propagation and USNC-URSI Radio Science Meeting, San Diego, CA, USA.

Abolfazl Haddadi received his M. Sc and Ph. D. degrees in electrical engineering from AmirKabir University of Technology (Tehran Polytechnique), Tehran, Iran, in 2010 and 2015, respectively. His Ph. D. thesis was entitled "Reflector Antenna Surface Distortion Determination and Compensation." He was an antenna engineer at Iranian Telecommunications Research Center (ITRC) and Iranian Space Research Center (ISRC) with focus on phased array and reflector antennas for space applications. In March 2015, he was at Chalmers University of Technology, Gteborg, Sweden, as a visiting researcher. Currently, he is a senior antenna engineer at GAPWAVES AB, Gteborg, Sweden. His main research interests include gap waveguide-based antennas, phased array antennas, and antenna industrialization methods for mass production.

Ashraf Uz Zaman (M'14) was born in Chittagong, Bangladesh. He received the B.Sc. degree in electrical and electronics engineering from the Chittagong University of Engineering and Technology, Chittagong. He received the M.Sc. and PhD degree from Chalmers University of Technology, Gteborg, Sweden, in 2007 and 2013 respectively. He is currently an assistant professor with the Communication and Antenna Division of the same university. His current research interests include millimeter wave high efficiency planar antennas in general, gap waveguide technology, frequency selective surfaces, microwave passive components, packaging techniques and integration of MMICs with the antennas.

Jian Yang (M'02SM'10) received the B.Sc. degree in electrical engineering from the Nanjing University of Science and Technology, Nanjing, China, in 1982, the M.Sc. degree in electrical engineering from the Nanjing Research Center of Electronic Engineering, Nanjing, in 1985, and the Swedish Licentiate and Ph.D. degrees from Chalmers University of Technology, Gothenburg, Sweden, in 1998 and 2001, respectively. From 1985 to 1996, he was with the Nanjing Research Institute of Electronics Technology, Nanjing, China, as a Senior Engineer. From 1999 to 2005, he was with the Department of Electromagnetics, Chalmers University of Technology, Gothenburg, Sweden, as a Research Engineer. During 2005 and 2006, he was with COMHAT AB as a Senior Engineer. From 2006 to 2010, he was an Assistant Professor, from 2010 to 2016, he was an Associate Professor, and since 2016 he has been a professor with the Department of Signals and Systems, Chalmers University of Technology. His research interests include 60-140GHz antennas, terahertz antennas, MIMO antennas, ultrawideband (UWB) antennas and UWB feeds for reflector antennas, UWB radar systems,UWB antennas in near-field sensing applications, hat-fed antennas, reflector antennas, radome design, and computational electromagnetics.

Herbert Zirath (M'86-SM'08-F'11) was born in Göteborg, Sweden, on March 20, 1955. He received the M. Sc and Ph. D. degree in electrical engineering from Chalmers University, Göteborg, Sweden, in 1980 and 1986, respectively. From 1986 to 1996 he was a researcher at the Radio and Space Science at Chalmers University, engaged in developing a GaAs and InP based HEMT technology, including devices, models and circuits. In the spring-summer 1998 he was research fellow at Caltech, Pasadena, USA, engaged in the design of MMIC frequency multipliers and Class E Power amplifiers. He is since 1996 Professor in High Speed Electronics at the Department of Microtechnology and Nanoscience, MC2, at Chalmers University. He became the head of the Microwave Electronics Laboratory 2001. At present he is leading a group of approximately 40 researchers in the area of high frequency semiconductor devices and circuits. His main research interests include MMIC designs for wireless communication and sensor applications based on III-V, III-N, Graphene, and silicon devices. He is author/co-author of more than 560 refereed journal/conference papers, h-index of 41, and holds 5 patents. He is research fellow at Ericsson AB, leading the development of a D-band (110-170 GHz) chipset for high data rate wireless communication. He is a co-founder of Gotmic AB, a company developing highly integrated front-end MMIC chip-sets for 60 GHz and E-band wireless communication.

Ahmed A. Kishk (S'84-M'86-SM'90-F'98) received the BS degree in Electronic and Communication Engineering from Cairo University, Cairo, Egypt, in 1977, and BSc. in Applied Mathematics from Ain-Shams University, Cairo, Egypt, in 1980. In 1983 and 1986, he received M. Eng., and Ph.D. degrees from the Department of Electrical Engineering, University of Manitoba, Winnipeg, Canada, respectively. In 1986, he joined the Department of Electrical Engineering, University of Mississippi, He was a Professor at the University of Mississippi (1995-2011). Currently, he is a Professor at Concordia University, Montréal, Québec, Canada (since 2011) as Tier 1 Canada Research Chair in Advanced Antenna Systems. He was the 2017 AP-S president.

His research interest includes the areas of millimeter wave antennas for 5G applications, Analog beamforming network, Antennass, microwave passive circuits and componenets, EBG, artificial magnetic conductors, phased array antennas, reflect/transmitarray, wearable antennas. He has published over 330-refereed Journal articles and 500 conference papers. He is a co-author of four books and several book chapters and the editor of three books.